




# Batagayite, $\text{CaZn}_2(\text{Zn,Cu})_6(\text{PO}_4)_4(\text{PO}_3\text{OH})_3 \cdot 12\text{H}_2\text{O}$ , a new phosphate mineral from Këster tin deposit (Yakutia, Russia): occurrence and crystal structure

Victor N. Yakovenchuk<sup>1</sup> · Yakov A. Pakhomovsky<sup>1</sup> · Nataliya G. Konopleva<sup>1</sup> · Taras L. Panikorovskii<sup>1,2</sup> · Ayya Bazai<sup>1</sup> · Julia A. Mikhailova<sup>1</sup> · Vladimir N. Bocharov<sup>3</sup> · Gregory Yu. Ivanyuk<sup>1</sup> · Sergey V. Krivovichev<sup>1,2</sup> 

Received: 30 June 2017 / Accepted: 1 December 2017 / Published online: 14 December 2017  
© Springer-Verlag GmbH Austria, part of Springer Nature 2017

## Abstract

Batagayite,  $\text{CaZn}_2(\text{Zn,Cu})_6(\text{PO}_4)_4(\text{PO}_3\text{OH})_3 \cdot 12\text{H}_2\text{O}$ , is a new secondary phosphate mineral from the Këster deposit, Arga-Ynnykh-Khai massif, NE Yakutia, Russia. It is monoclinic,  $P2_1$ ,  $a = 8.4264(4)$ ,  $b = 12.8309(6)$ ,  $c = 14.6928(9)$  Å,  $\beta = 98.514(6)^\circ$ ,  $V = 1571.05(15)$  Å<sup>3</sup> and  $Z = 2$  (from single-crystal X-ray diffraction data). Batagayite crystals are blades up to 2 mm long, flattened on {001} and elongated on [100]; blades often grow in radial aggregates. Associated minerals are arsenolite, native copper, epifanovite, fluorapatite, libethenite, Na-analogue of batagayite, pseudomalachite, quartz, sampleite, tobermorite, and Mg-analogue of hopeite. The streak is white and the luster is vitreous. The mineral is brittle and has a perfect cleavage on {001}, no parting was observed. The Mohs hardness is 3. Density, determined by the float-sink method in Clerici solution, is 2.90(3) g/cm<sup>3</sup>, and the calculated density is 3.02 g/cm<sup>3</sup> (using the empirical formula and single-crystal unit-cell parameters). Batagayite is biaxial, optically negative,  $\alpha = 1.566 \pm 0.002$ ,  $\beta = 1.572 \pm 0.002$ ,  $\gamma = 1.573 \pm 0.002$  at 589 nm.  $2V_{\text{meas.}} = 40(5)^\circ$ ,  $2V_{\text{calc.}} = 44.3^\circ$ . Optical orientation:  $Z$  is perpendicular to (001), further details unclear. No dispersion or pleochroism were observed. The mean chemical composition determined by electron microprobe is: Na<sub>2</sub>O 0.31, MgO 1.39, Al<sub>2</sub>O<sub>3</sub> 0.55, SiO<sub>2</sub> 0.48, P<sub>2</sub>O<sub>5</sub> 34.37, K<sub>2</sub>O 0.17, CaO 2.76, MnO 1.03, CuO 5.80, ZnO 35.62, CdO 0.24 wt%. The H<sub>2</sub>O content estimated from the crystal-structure refinement is 16.83 wt%, giving a total of 99.55 wt%. The empirical formula calculated on the basis of P + Si = 7 is  $(\text{Zn}_{6.22}\text{Cu}_{1.04}\text{Ca}_{0.70}\text{Mg}_{0.49}\text{Mn}_{0.21}\text{Al}_{0.15}\text{Na}_{0.14}\text{K}_{0.05}\text{Cd}_{0.03})_{\Sigma 9.03}(\text{P}_{6.89}\text{Si}_{0.11})_{\Sigma 7.00}\text{O}_{24.91}(\text{OH})_{3.09} \cdot 12.10\text{H}_2\text{O}$ . The mineral easily dissolves in 10% room-temperature HCl. The eight diagnostic lines in the X-ray powder-diffraction pattern are ( $I$ - $d$ [Å]- $hkl$ ): 100-14.59-001, 25-6.34-012, 11-6.02-111, 37-4.864-003, 13-4.766-112, 20-3.102-1  $\bar{2}$   $\bar{4}$ , 11-2.678-2  $\bar{3}$   $\bar{3}$ , 16-2.411-044. The crystal structure of batagayite was solved by direct methods and refined to  $R_1 = 0.069$  for 3847 independent reflections with  $F_o > 4\sigma(F_o)$ . It is based upon complex heteropolyhedral  $[\text{M}_8(\text{PO}_4)_4(\text{PO}_3\text{OH})_3(\text{H}_2\text{O})_9]^{2-}$  layers parallel to the (001) plane. The layer can be considered as consisting of three sublayers, one **A** and two **B**. The central **A** layer has the composition  $[\text{M}_4(\text{PO}_4)_4(\text{H}_2\text{O})_4]^{4-}$  and consists of the zigzag chains of edge-sharing ( $\text{MO}_6$ ) octahedra running parallel to the  $a$  axis and linked into layers by sharing peripheral O atoms. The ( $\text{PO}_4$ ) tetrahedra are attached above and below the holes created by the linkage of zigzag octahedral chains. The **B** sublayer consists of chains of ( $\text{ZnO}_4$ ) and ( $\text{PO}_3\text{OH}$ ) tetrahedra. The interlayer space is occupied by the  $\text{Ca}^{2+}$  cations and  $\text{H}_2\text{O}$  molecules. Batagayite is a secondary low-temperature mineral formed as a result of alteration of primary minerals such as native copper and fluorapatite. On the basis of its structural complexity calculated as 1058.257 bits/cell (taking into account contributions from H atoms), batagayite should be considered as a very complex mineral. The high complexity of batagayite is due to its high hydration state and the modular character of its structure, which contains both octahedral-tetrahedral layers and tetrahedral chains.

**Keywords** Batagayite · New mineral · Calcium-zinc-copper phosphate · Këster deposit · Yakutia

Editorial handling: M. A.T.M. Broekmans

✉ Sergey V. Krivovichev  
s.krivovichev@spbu.ru

Extended author information available on the last page of the article

## Introduction

The Këster deposit is a greisen-type Sn-Ta deposit located in the north-east part of Yakutia and discovered in 1937 by P.P. Epifanov. Këster is a type locality for kësterite,

$\text{Cu}_2\text{ZnSnS}_4$  (Ivanov and Pyatenko 1959), which is known for the applications of its synthetic analogues in solar-cell technologies (Liu et al. 2016). The deposit has a diverse and rich secondary phosphate mineralization that includes ambligonite, augelite, libethenite, pseudomalachite, turquoise, and other minerals (Kokunin 2011). Recently, we have described epifanovite,  $\text{NaCaCu}_5(\text{PO}_4)_4[\text{AsO}_2(\text{OH})_2] \cdot 7\text{H}_2\text{O}$  (Yakovenchuk et al. 2017; Panikorovskii et al. 2017), the first new phosphate mineral species from K ester. Epifanovite belongs to the lavendulan group and occurs in association with sampleite,  $\text{NaCaCu}_5(\text{PO}_4)_4\text{Cl} \cdot 5\text{H}_2\text{O}$  (Giester et al. 2007; Panikorovskii et al., in preparation). Herein, we report on the occurrence, composition, properties and crystal structure of batagayite,  $\text{CaZn}_2(\text{Zn,Cu})_6(\text{PO}_4)_4(\text{PO}_3\text{OH})_3 \cdot 12\text{H}_2\text{O}$ , the second new phosphate from the K ester deposit. The mineral is named in honor of Batagay, a small town located ca. 50 km from the deposit. Currently, Batagay is an administrative center of the Verhoyansk ulus of the Sakha Republic, Russia.

The new mineral and its name were approved by the Commission on New Minerals, Nomenclature and Classification of the International Mineralogical Association (IMA CNMNC; proposal 2017-002). The holotype specimen is deposited in the collections of the Mineralogical Museum of St. Petersburg State University, Russia, under catalogue number 19,659/1.

## Occurrence

The mineral was found in a quartz-phosphate nest (about 5 m in diameter) within greisenized cassiterite-bearing granodiorite of the K ester deposit (Arga-Ynnykh-Khai massif, NE Yakutia, Russia). The nest consists of pale-grey botryoidal aggregates of fluorapatite (up to 30 cm in diameter) and porous milky-white aggregates of quartz (up to 10 cm in diameter). Walls of numerous voids and fractures in these aggregates are incrustated by dark-green crystals and spherulites (up to 5 mm) of dark green pseudomalachite and light blue sampleite, druses of pale-green long-prismatic crystals of libethenite (up to 7 mm long), and separated clusters of native copper (up to 3 mm in diameter). Radial aggregates of colorless flattened-prismatic crystals of batagayite (up to 2 mm long, Fig. 1) grow on the surface of copper clusters in close association with colorless cubo-octahedral crystals of arsenolite (up to 1 mm in diameter), colorless tetragonal plates of tobermorite (up to 1 mm in diameter), turquoise-blue crusts of an epifanovite (up to 50  $\mu\text{m}$  thick) and radial fibrous aggregates of unknown mineral (up to 3 mm in diameter). Other associated minerals are libethenite, Na-analogue of batagayite and Mg-analogue of hopeite.

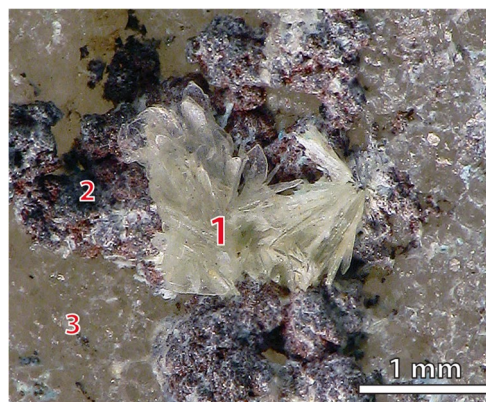


Fig. 1 Radiated aggregates of batagayite (1) on copper cluster (2) growing on fluorapatite (3)

## Appearance and physical properties

Batagayite crystals are blades up to 2 mm long, flattened on {001} and elongated on [100]; blades often grow in radial aggregates (Fig. 1). The streak is white and the luster is vitreous. The mineral is brittle and has a perfect cleavage on {001}, no parting was observed. The Mohs hardness is 3. Density, determined by the float-sink method in Clerici solution, is  $2.90(3) \text{ g/cm}^3$ , and the calculated density is  $3.02 \text{ g/cm}^3$  (using the empirical formula and single-crystal unit-cell parameters). The observed difference between the measured and calculated density values is most probably caused by admixtures of mineral phases with lower density.

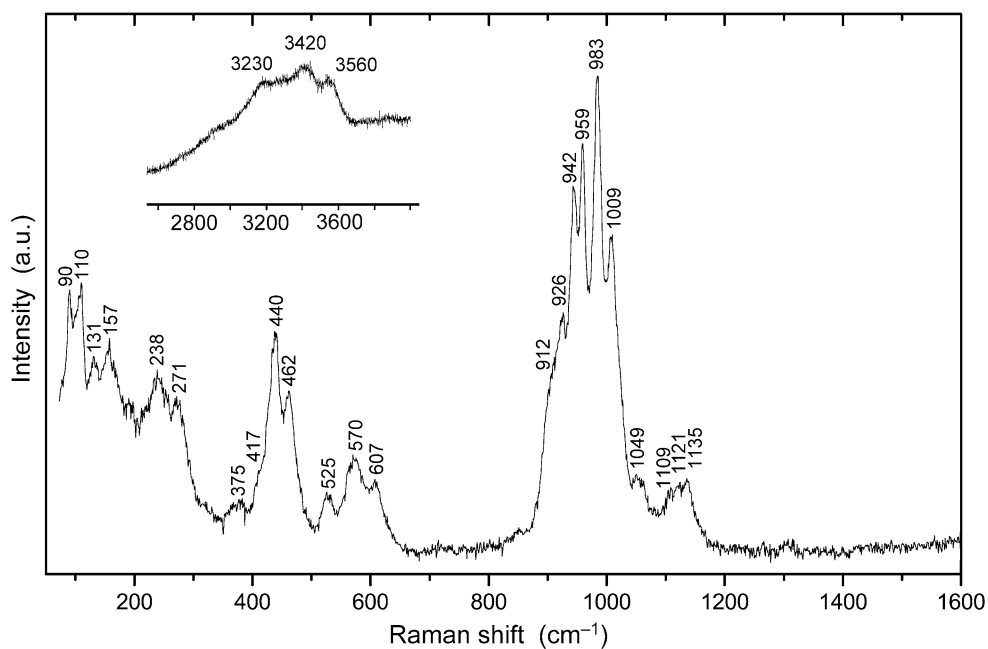
Batagayite is biaxial, optically negative,  $\alpha = 1.566 \pm 0.002$ ,  $\beta = 1.572 \pm 0.002$ ,  $\gamma = 1.573 \pm 0.002$  at 589 nm.  $2V_{\text{meas}} = 40(5)^\circ$ ,  $2V_{\text{calc}} = 44.3^\circ$ . Optical orientation: Z is perpendicular

Table 1 Chemical composition of batagayite (wt%)

	Mean	Range	SD*	Calibrant material
$\text{Na}_2\text{O}$	0.31	0.00–0.61	0.43	Lorenzenite
$\text{MgO}$	1.39	1.38–1.41	0.02	Pyrope
$\text{Al}_2\text{O}_3$	0.55	0.07–1.04	0.69	Pyrope
$\text{SiO}_2$	0.48	0.14–0.82	0.48	Wollastonite
$\text{P}_2\text{O}_5$	34.37	33.60–35.14	1.09	Fluorapatite
$\text{K}_2\text{O}$	0.17	0.17–0.17	0.00	Wadeite
$\text{CaO}$	2.76	1.59–3.93	1.66	Wollastonite
$\text{MnO}$	1.03	0.49–1.56	0.75	$\text{MnCO}_3$
$\text{CuO}$	5.80	3.77–7.83	2.87	Copper
$\text{ZnO}$	35.62	35.48–35.75	0.19	Sphalerite
$\text{CdO}$	0.24	0.00–0.48	0.34	CdSe
$\text{H}_2\text{O}^*$	16.83			
Total	99.55			

\*SD = standard deviation

\*\* Calculated from the crystal-structure data

**Fig. 2** Raman spectrum of batagayite

to (001), further details unclear. No dispersion or pleochroism were observed.

The mean chemical composition of batagayite corresponds to the following empirical formula (calculated on the basis of P + Si = 7): (Zn<sub>6.22</sub>Cu<sub>1.04</sub>Ca<sub>0.70</sub>Mg<sub>0.49</sub>Mn<sub>0.21</sub>A

## Chemical composition

The chemical composition of batagayite was determined using a Cameca MS-46 electron probe micro-analyzer [WDS (wavelength dispersive spectroscopy) mode, 20 kV, 20–30 nA, 10 μm beam diameter]. The mean analytical results of two different crystals (12 points) are given in Table 1. The H<sub>2</sub>O content was calculated on the basis of the crystal-structure refinement (see below).

**Table 2** Raman bands in the batagayite spectrum and their interpretation

Raman shift (cm <sup>-1</sup> )	Assignment	Type
3230sh, 3420, 3560	OH	$\nu_1, \nu_3$
959 s, 942, 926, 912sh	PO <sub>4</sub>	$\nu_1$
983 s, 1009s, 1049, 1109w, 1121w, 1135w	PO <sub>4</sub>	$\nu_3$
417sh, 440, 462	PO <sub>4</sub>	$\nu_2$
607	PO <sub>4</sub>	$\nu_4$
525, 570	ZnO <sub>6</sub>	$\nu_1, \nu_2$
157, 238	ZnO <sub>6</sub>	$\nu_3, \nu_4$
271, 375w	ZnO <sub>4</sub>	$\nu_1, \nu_2$
90, 110, 131	ZnO <sub>4</sub>	$\nu_3, \nu_4$

sh, shoulder; s, strong intensity; w, weak

**Table 3** Crystal data and structure refinement for batagayite

Temperature (K)	293(2)
Crystal system	monoclinic
Space group	$P2_1$
$a$ (Å)	8.4264(4)
$b$ (Å)	12.8309(6)
$c$ (Å)	14.6928(9)
$\beta$ (°)	98.514(6)
$V$ (Å <sup>3</sup> )	1571.05(15)
$Z$	2
$\rho_{\text{calc}}$ (g·cm <sup>-3</sup> )	2.967
$\mu$ (mm <sup>-1</sup> )	6.509
$F(000)$	1353.0
Crystal size (mm <sup>3</sup> )	0.12 × 0.08 × 0.001
Radiation	MoK $\alpha$ ( $\lambda = 0.71073$ Å)
2 $\theta$ range for data collection (°)	6.148 to 50
Index ranges	$-10 \leq h \leq 8, -15 \leq k \leq 15, -13 \leq l \leq 17$
Reflections collected	7310
Independent reflections	4837 [ $R_{\text{int}} = 0.0550, R_{\text{sigma}} = 0.0679$ ]
Data/restraints/parameters	4835/1/479
Goodness-of-fit on $F^2$	1.045
Final R indexes [ $I \geq 2\sigma(I)$ ]	$R_1 = 0.069, wR_2 = 0.186$
Final R indexes [all data]	$R_1 = 0.074, wR_2 = 0.189$
Largest diff. peak/hole ( $e \cdot \text{Å}^{-3}$ )	2.79/-1.25
Flack parameter	0.05(2)

**Table 4** Atomic coordinates, occupancies, bond-valence sums (BVS, valence units\*) and equivalent isotropic displacement parameters of batagayite

Atom	Occupancy	BVS	<i>O</i>	<i>y</i>	<i>z</i>	<i>U</i> <sub>eq</sub>
Ca	Ca	1.95	0.5447(6)	0.3297(4)	0.3746(3)	0.0189(11)
M1	Zn	2.09	0.4257(3)	0.3909(2)	0.71823(19)	0.0162(7)
M2	Zn	1.95	0.9757(3)	0.4902(2)	0.71040(19)	0.0163(7)
M3	Zn	1.85	0.2814(3)	0.0657(2)	0.9841(2)	0.0179(7)
M4	Zn <sub>0.87</sub> Mg <sub>0.13</sub>	1.94	0.1789(3)	0.8000(2)	0.9887(2)	0.0150(12)
M5	Cu <sub>0.50</sub> Zn <sub>0.50</sub>	1.92	0.1078(3)	0.8158(2)	0.7480(2)	0.0172(7)
M6	Zn	1.99	0.6815(3)	0.0677(2)	0.9862(2)	0.0196(7)
M7	Cu <sub>0.50</sub> Zn <sub>0.32</sub> Mg <sub>0.18</sub>	1.90	0.5957(4)	0.0589(3)	0.7471(2)	0.0172(12)
M8	Zn	2.00	0.7815(3)	0.8001(2)	0.9805(2)	0.0169(7)
P1	P	4.89	0.4676(7)	0.2353(5)	0.8774(5)	0.0146(14)
P2	P	4.82	0.4410(7)	0.8978(5)	0.8695(4)	0.0133(13)
P3	P	4.80	0.9703(7)	0.6351(5)	0.8734(4)	0.0122(13)
P4	P	4.91	0.9458(7)	0.9688(5)	0.8714(4)	0.0141(13)
P5	P	4.91	0.2870(7)	0.6136(5)	0.6743(4)	0.0159(13)
P6	P	5.02	0.6649(7)	0.4260(5)	0.5883(4)	0.0177(13)
P7	P	4.94	0.1064(8)	0.2723(5)	0.6616(5)	0.0183(13)
O <sub>W</sub> 1	H <sub>2</sub> O	0.24	0.5233(18)	0.1091(13)	0.0892(12)	0.015(4)
O <sub>W</sub> 2	H <sub>2</sub> O	0.49	0.6958(18)	-0.0481(15)	0.6564(12)	0.019(4)
O <sub>W</sub> 3	H <sub>2</sub> O	0.59	0.760(2)	-0.0646(13)	0.0678(11)	0.015(4)
O <sub>W</sub> 4	H <sub>2</sub> O	0.58	0.258(2)	0.9311(13)	1.0723(12)	0.018(4)
O <sub>W</sub> 5	H <sub>2</sub> O	0.35	0.755(2)	0.1743(15)	0.7165(14)	0.026(4)
O <sub>W</sub> 6	H <sub>2</sub> O	0.13	0.948(2)	0.7540(18)	0.6025(15)	0.032(5)
O <sub>W</sub> 7	H <sub>2</sub> O	0.31	0.370(2)	0.2608(16)	0.4734(13)	0.029(4)
O <sub>W</sub> 8	H <sub>2</sub> O	0.00	0.926(2)	0.0257(13)	0.5498(13)	0.025(4)
O <sub>W</sub> 9	H <sub>2</sub> O	0.33	0.3565(19)	0.2372(13)	0.2703(11)	0.015(3)
O <sub>W</sub> 10	H <sub>2</sub> O	0.31	0.017(2)	0.7525(17)	0.0963(14)	0.028(4)
O <sub>W</sub> 11	H <sub>2</sub> O	0.44	0.182(2)	0.9243(16)	0.6502(13)	0.028(5)
O <sub>W</sub> 12	H <sub>2</sub> O	0.26	0.436(2)	0.0889(17)	0.6171(13)	0.030(5)
O11	O	1.71	0.4499(19)	0.1672(13)	0.7923(11)	0.014(4)
O12	O	2.00	0.3300(19)	0.2110(13)	0.9311(12)	0.014(4)
O13	O	1.96	0.6286(18)	0.2153(14)	0.9391(12)	0.0142(14)
O14	O	1.58	0.4586(17)	0.3553(14)	0.8482(12)	0.0142(14)
O21	O	1.84	0.454(2)	0.9343(14)	0.7712(11)	0.017(4)
O22	O	1.64	0.571(2)	0.8140(17)	0.8981(12)	0.023(4)
O23	O	1.94	0.4658(17)	0.9919(14)	0.9369(11)	0.0142(14)
O24	O	1.83	0.2720(18)	0.8515(14)	0.8749(12)	0.018(4)
O31	O	1.70	0.9699(19)	0.6999(14)	0.7864(13)	0.018(4)
O32	O	1.93	0.8244(19)	0.6562(14)	0.9223(12)	0.019(4)
O33	O	1.92	0.1271(18)	0.6524(14)	0.9418(11)	0.013(3)
O34	O	1.54	0.9696(17)	0.5160(13)	0.8431(11)	0.0142(14)
O41	O	1.75	0.0743(19)	0.0499(15)	0.9037(11)	0.017(4)
O42	O	1.66	0.9508(18)	0.9290(14)	0.7736(12)	0.0142(14)
O43	O	2.02	0.9645(18)	0.8773(15)	0.9397(12)	0.018(4)
O44	O	1.73	0.7746(18)	0.0177(13)	0.8707(11)	0.011(3)
O51	O	1.79	0.387(2)	0.5383(13)	0.7392(11)	0.018(4)
O52	O	1.96	0.283(2)	0.7236(13)	0.7125(11)	0.015(4)
O53	O	1.74	0.1186(19)	0.5686(14)	0.6430(11)	0.017(3)
O <sub>h</sub> 54**	OH	1.24	0.374(2)	0.6310(14)	0.5867(11)	0.021(4)
O61	O	1.92	0.7940(16)	0.5047(13)	0.6148(11)	0.0142(14)
O62**	O	1.38	0.5155(19)	0.4700(15)	0.5306(13)	0.027(4)
O63	O	1.79	0.6255(19)	0.3661(15)	0.6724(13)	0.024(4)

**Table 4** (continued)

Atom	Occupancy	BVS	<i>O</i>	<i>y</i>	<i>z</i>	<i>U</i> <sub>eq</sub>
O <sub>h</sub> 64**	OH	1.32	0.7257(19)	0.3404(15)	0.5226(11)	0.023(4)
O71**	O	1.32	-0.012(2)	0.2508(15)	0.5759(12)	0.023(4)
O72	O	1.74	0.042(2)	0.3432(13)	0.7313(12)	0.022(4)
O73	O	1.76	0.2659(19)	0.3166(15)	0.6376(12)	0.022(4)
O <sub>h</sub> 74	OH	1.14	0.144(2)	0.1642(15)	0.7099(13)	0.026(4)

\*Calculated using bond-valence parameters provided by Gagné and Hawthorne (2015)

\*\*The O<sub>h</sub>64-O71 and O<sub>h</sub>54-O62 pairs of atoms are involved in strong hydrogen bonds (see text for details)

I<sub>0.15</sub>Na<sub>0.14</sub>K<sub>0.05</sub>Cd<sub>0.03</sub>)<sub>Σ9.03</sub>(P<sub>6.89</sub>Si<sub>0.11</sub>)<sub>Σ7.00</sub>O<sub>24.91</sub>(OH)<sub>3.09</sub>·12·10H<sub>2</sub>O. Taking into account the results of crystal-structure study, the formula can be re-written as (Ca<sub>0.70</sub>Na<sub>0.14</sub>Mg<sub>0.11</sub>K<sub>0.05</sub>)<sub>Σ1.00</sub>Zn<sub>2</sub>(Zn<sub>3.97</sub>Cu<sub>1.04</sub>Mg<sub>0.38</sub>Zn<sub>0.25</sub>Mn<sub>0.21</sub>Al<sub>0.15</sub>Cd<sub>0.03</sub>)<sub>Σ6.03</sub>(P<sub>6.89</sub>Si<sub>0.11</sub>)<sub>Σ7.00</sub>O<sub>20.91</sub>(OH)<sub>3.09</sub>·12·10H<sub>2</sub>O. The simplified formula is CaZn<sub>2</sub>(Zn,Cu)<sub>6</sub>(PO<sub>4</sub>)<sub>4</sub>(PO<sub>3</sub>OH)<sub>3</sub>·12H<sub>2</sub>O and the end-member formula is CaZn<sub>2</sub>Zn<sub>6</sub>(PO<sub>4</sub>)<sub>4</sub>(PO<sub>3</sub>OH)<sub>3</sub>·12H<sub>2</sub>O, which requires (in wt.%) CaO 3.87, ZnO 44.99, P<sub>2</sub>O<sub>5</sub> 34.33, H<sub>2</sub>O 16.81, sum 100.00. The mineral easily dissolves in 10% room-temperature HCl.

### Raman spectroscopy

Raman spectrum of batagayite (Fig. 2) was obtained using a Horiba Jobin–Yvon LabRam HR 800 spectrometer (wavelength 514 nm), which is equipped with a 50× (NA 0.75) objective. The sample was measured with 8 mW laser power. The most intensive bands (Table 2) at 983, 959, 942, 1009 and 926 as well as the shoulder at 912 cm<sup>-1</sup> correspond to the symmetric and antisymmetric stretching modes vibrations of the phosphate anion, PO<sub>4</sub><sup>3-</sup>, other intensive bands at 440, 462 cm<sup>-1</sup> can be assigned to the bending vibrations of the same bonds (Frost et al. 2014). According to the DFT calculations (Rudolph and Irmer 2007), the high-frequency bands can be related to PO<sub>4</sub><sup>3-</sup> groups coordinated by H<sub>2</sub>O molecules. Other Raman bands in the range 1100–1150 cm<sup>-1</sup> can be attributed to the antisymmetric stretching vibrations ν<sub>3</sub> of the PO<sub>4</sub><sup>3-</sup> groups. By analogy with minerals with similar chemical compositions, the bands at 90, 110, 131, 157, 238, 271, 375 (weak), 525, 570 cm<sup>-1</sup> (Frost 2004; Frost et al. 2007) can be related to the different vibration modes of the Zn–O and Cu–O bonds. The broad bands in the range 3200–3600 cm<sup>-1</sup> are attributed to stretching vibrations of the O–H bonds, which can be related to molecular H<sub>2</sub>O and hydroxyl groups.

### Crystal structure

#### Experimental

The single-crystal X-ray diffraction experiment was carried out using an Agilent Technologies Xcalibur Eos

diffractometer operated at 50 kV and 40 mA. A hemisphere of three-dimensional data was collected at room temperature using monochromatic MoK<sub>α</sub> X-radiation with frame widths of 1° and 150 s count for each frame. Since the crystals of batagayite are very thin plates, selection of the appropriate material for the single-crystal study was difficult. Two crystals were studied, one of which produced a doubled *c* unit-cell parameter, due to the pseudo-rhombohedral twinning on (001) with partial overlap of reflections from two twin domains. The data used for the structure refinement were obtained from a second crystal, which showed only minor signs of pseudomerohedral twinning. The intensity data were reduced and corrected for Lorentz, polarization and background effects. Empirical absorption correction was applied in the CrysAlisPro (Agilent Technologies 2014) program complex using spherical harmonics, implemented in the SCALE3 ABSPACK scaling algorithm. The crystal structure was solved by direct methods with the SHELX program package (Sheldrick 2008) and refined to *R*<sub>1</sub> = 0.069 for 3847 independent reflections with *F*<sub>o</sub> > 4σ(*F*<sub>o</sub>). In the final refinement, 21 reflections were omitted, which showed strong disagreement between observed and calculated structure factors, most probably due to the influence of pseudo-merohedral twinning. The quality of the diffraction data did not allow the location of H sites in the structure. Crystal data, data collection information and structure refinement details are given in Table 3, atom coordinates, bond-valence sums and selected interatomic distances are in Tables 4 and 5, respectively. Anisotropic displacement parameters and other details of structure refinement are deposited as a supplementary CIF (Crystallographic Information File).

### Structure description

The crystal structure of batagayite (Fig. 3) belongs to a new structure type for minerals and inorganic compounds. It contains nine cation positions (Fig. 4). There is one Ca site coordinated by eight O atoms with the Ca–O distances in the range 2.357–2.679 Å and one O atom resided at 2.95 Å. There are two tetrahedrally coordinated sites, *M*1 and *M*2,

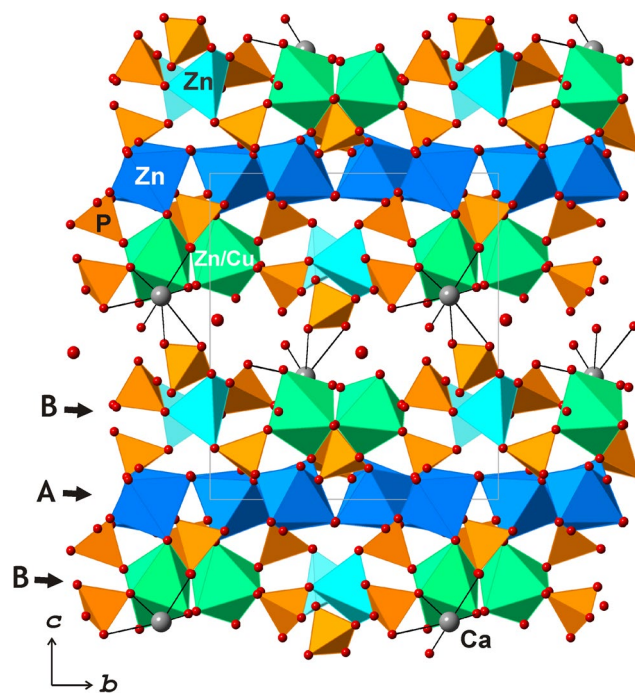


**Table 5** Selected interatomic distances (Å) for the crystal structure of batagayite

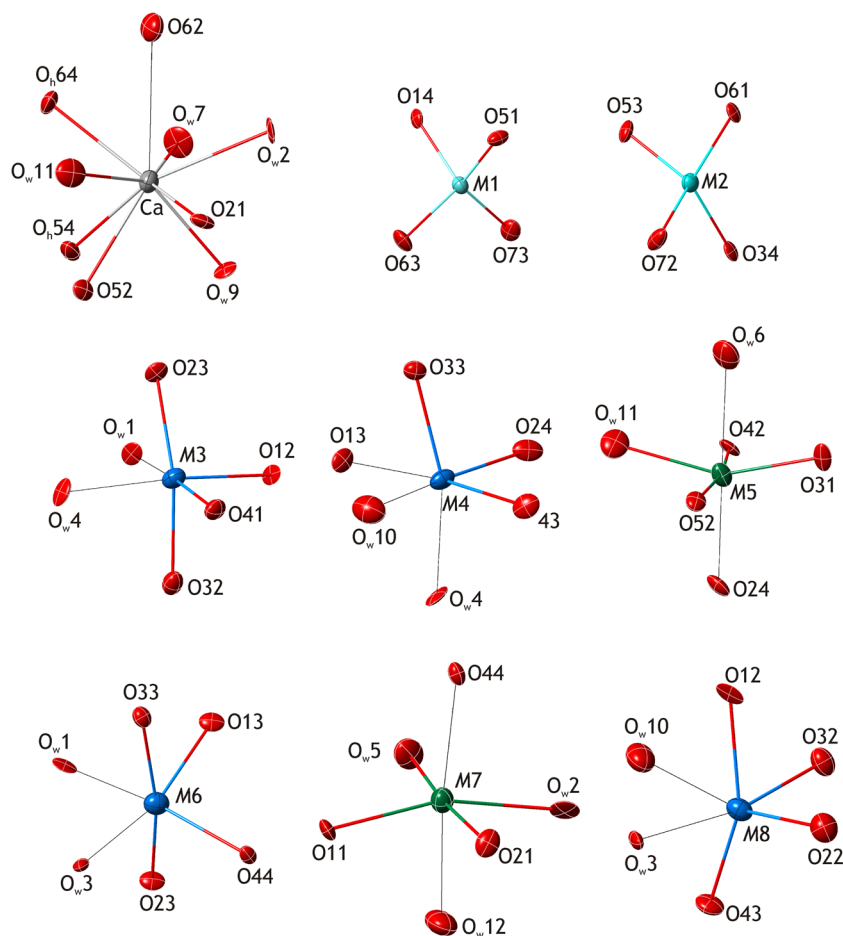
Bond	Distance	Bond	Distance	Bond	Distance
M1-O73	1.911(17)	M5-O52	2.019(17)	P2-O21	1.537(17)
M1-O63	1.930(16)	M5-O31	2.019(18)	P2-O22	1.55(2)
M1-O14	1.943(17)	M5-O42	2.037(17)	P2-O23	1.556(19)
M1-O51	1.952(17)	M5-O <sub>w</sub> 11	2.16(2)	P2-O24	1.556(17)
<M1-O>	1.934	M5-O24	2.199(17)	<P2-O>	1.550
		M5-O <sub>w</sub> 6	2.48(2)		
M2-O61	1.927(15)	<M5-O>	2.152	P3-O31	1.524(19)
M2-O53	1.949(16)			P3-O32	1.537(18)
M2-O72	1.977(17)	M6-O13	2.042(18)	P3-O33	1.553(17)
M2-O34	1.986(17)	M6-O44	2.075(15)	P3-O34	1.591(18)
<M2-O>	1.960	M6-O23	2.094(15)	<P3-O>	1.551
		M6-O33	2.096(17)		
Ca-O <sub>w</sub> 9	2.357(16)	M6-O <sub>w</sub> 3	2.125(18)	P4-O41	1.53(2)
Ca-O <sub>w</sub> 7	2.386(17)	M6-O <sub>w</sub> 1	2.223(17)	P4-O42	1.531(18)
Ca-O <sub>h</sub> 64	2.468(16)	<M6-O>	2.109	P4-O43	1.538(19)
Ca-O52	2.480(17)			P4-O44	1.572(16)
Ca-O21	2.530(18)	M7-O11	2.031(16)	<P4-O>	1.543
Ca-O <sub>w</sub> 2	2.550(17)	M7-O21	2.057(17)		
Ca-O <sub>w</sub> 11	2.68(2)	M7-O <sub>w</sub> 5	2.090(18)	P5-O51	1.521(18)
Ca-O <sub>h</sub> 54	2.679(19)	M7-O <sub>w</sub> 2	2.169(19)	P5-O52	1.521(17)
Ca-O62	2.95(2)	M7-O <sub>w</sub> 12	2.203(18)	P5-O53	1.537(17)
<Ca-O>	2.564	M7-O44	2.244(16)	P5-O <sub>h</sub> 54	1.588(17)
		<M7-O>	2.132	<P5-O>	1.542
M3-O41	1.968(17)				
M3-O23	2.027(16)	M8-O43	1.998(16)	P6-O61	1.493(16)
M3-O12	2.084(17)	M8-O22	1.999(18)	P6-O62	1.519(18)
M3-O32	2.097(18)	M8-O12	2.058(17)	P6-O63	1.532(19)
M3-O <sub>w</sub> 4	2.186(17)	M8-O32	2.089(18)	P6-O <sub>h</sub> 64	1.597(19)
M3-O <sub>w</sub> 1	2.433(16)	M8-O <sub>w</sub> 3	2.182(17)	<P6-O>	1.535
<M3-O>	2.133	M8-O <sub>w</sub> 10	2.49(2)		
		<M8-O>	2.136	P7-O71	1.514(18)
M4-O33	2.041(18)			P7-O72	1.529(17)
M4-O24	2.059(18)	P1-O11	1.515(18)	P7-O73	1.547(17)
M4-O43	2.093(17)	P1-O12	1.528(17)	P7-O <sub>h</sub> 74	1.57(2)
M4-O13	2.104(16)	P1-O13	1.537(16)	<P7-O>	1.540
M4-O <sub>w</sub> 4	2.132(17)	P1-O14	1.597(18)		
M4-O <sub>w</sub> 10	2.315(19)	<P1-O>	1.544		
<M4-O>	2.124				
O <sub>w</sub> 1-O51	2.68(2)	O <sub>w</sub> 4-O34	2.67(2)	O <sub>w</sub> 10-O41	2.71(3)
O <sub>w</sub> 1-O22	2.76(3)	O <sub>w</sub> 4-O14	2.68(2)	O <sub>w</sub> 10-O72	2.90(3)
O <sub>w</sub> 1-O13	2.84(2)	O <sub>w</sub> 5-O63	2.73(2)	O <sub>w</sub> 10-O12	2.94(4)
O <sub>w</sub> 2-O42	2.56(2)	O <sub>w</sub> 6-O <sub>w</sub> 7	2.75(3)	O <sub>w</sub> 11-O21	2.69(3)
O <sub>w</sub> 2-O12	2.80(3)	O <sub>w</sub> 6-O71	2.75(3)	O <sub>w</sub> 12-O62	2.73(2)
O <sub>w</sub> 2-O <sub>w</sub> 8	2.83(2)	O <sub>w</sub> 8-O <sub>w</sub> 11	2.75(3)	O <sub>h</sub> 64-O71	2.51(2)
O <sub>w</sub> 3-O14	2.58(2)	O <sub>w</sub> 8-O <sub>w</sub> 53	2.86(2)	O <sub>h</sub> 54-O62	2.58(3)
O <sub>w</sub> 3-O34	2.66(2)	O <sub>w</sub> 9-O31	2.79(2)	O <sub>h</sub> 74-O11	2.68(2)
O <sub>w</sub> 3-O43	2.83(2)	O <sub>w</sub> 9-O22	2.81(2)		

both fully occupied by Zn. There are six octahedrally coordinated sites, *M3-M8*, with variable degrees of geometrical distortion. For these sites, the *M-O* distances lie in the range from 1.968 to 2.490 Å. The *M4* and *M7* sites were refined with joint occupancies based upon their scattering powers, which allowed us to assign to these sites some quantity of Mg, in general agreement with the results of the chemical analyses (see the empirical formula above). Cu was assigned to the *M5* and *M7* sites because their coordination geometries, with two long *trans*-bonds, exhibit the Jahn–Teller distortion typical of Cu<sup>2+</sup> coordination (Jahn and Teller 1937). In addition, these sites play the same crystal chemical function, as they are located outside the dense octahedral-tetrahedral layer (see below). All other *M* sites possess elongated *M-O* bonds as well, but they are in *cis*- rather than in *trans*-orientations relative to each other (Fig. 4), which does not satisfy the geometrical conditions of a Jahn–Teller distortion.

The crystal structure contains seven P sites each tetrahedrally coordinated by four O atoms. The mean <P-O> bond lengths vary from 1.535 to 1.551 Å, in good agreement with the average distance of 1.537 Å provided for phosphates by Huminicki and Hawthorne (2002). Each of the P5O<sub>4</sub>, P6O<sub>4</sub> and P7O<sub>4</sub> tetrahedra possess three P-O bonds in the range 1.493–1.547 Å and one long P-O bond of 1.570–1.597 Å that is indicative of protonation of the respective O atoms and formation of the (PO<sub>3</sub>OH)<sup>2-</sup> groups. The P-O<sub>h</sub> distances observed in the crystal structure of batagayite are in

**Fig. 3** The crystal structure of batagayite viewed along the *a* axis

**Fig. 4** Coordination of cations in the crystal structure of batagayite.  $M$ -O bonds longer than 2.18 Å are shown as stick bonds



agreement with the average value of 1.581 Å provided by Ferraris and Ivaldi (1984).

The crystal structure of batagayite is based upon complex heteropolyhedral layers parallel to the (001) plane. The layer can be considered as consisting of three sublayers, one **A** and two **B**. The central layer (denoted as **A** in Fig. 3) has the composition  $[\text{M}_4(\text{PO}_4)_4(\text{H}_2\text{O})_4]^{4-}$  and is formed by the coordination polyhedra of *M3*, *M4*, *M6*, *M8*, *P1*, *P2*, *P3*, and *P4* atoms. It consists of zigzag chains of edge-sharing ( $\text{MO}_6$ ) octahedra running parallel to the *a* axis and linked into layers by sharing peripheral O atoms (Fig. 5a). The ( $\text{PO}_4$ ) tetrahedra are attached above and below the holes created by the linkage of zigzag octahedral chains. The **B** sublayer consists of chains of ( $\text{M1O}_4$ ), ( $\text{M2O}_4$ ), ( $\text{P5O}_3\text{OH}$ ), ( $\text{P6O}_3\text{OH}$ ), and ( $\text{P7O}_3\text{OH}$ ) tetrahedra. The ( $\text{MO}_4$ ) tetrahedra and ( $\text{P5O}_3\text{OH}$ ) and ( $\text{P7O}_3\text{OH}$ ) tetrahedra share corners to form four-membered rings, which are further linked via ( $\text{P6O}_3\text{OH}$ ) tetrahedra into chains parallel to the *a*

axis (Fig. 5b). The ( $\text{M5O}_6$ ) and ( $\text{M7O}_6$ ) octahedra are located in between the chains; these are the octahedra that are occupied by the  $\text{Cu}^{2+}$  cations (see discussion above). The complex **BAB** layers have the composition  $[\text{M}_8(\text{PO}_4)_4(\text{PO}_3\text{OH})_3(\text{H}_2\text{O})_9]^{2-}$  ( $M = \text{Zn}, \text{Cu}, \text{Mg}$ ). The  $\text{Ca}^{2+}$  cations and  $\text{H}_2\text{O}_{27}$ ,  $\text{H}_2\text{O}_{33}$ , and  $\text{H}_2\text{O}_{35}$  groups are located in the interlayer. The  $\text{H}_2\text{O}_{27}$  and  $\text{H}_2\text{O}_{35}$  molecules are bonded to Ca, whereas the  $\text{H}_2\text{O}_{33}$  group is held in the structure by hydrogen bonds only.

The quality of diffraction data did not allow for identification of the positions of the H atoms. However, the hydrogen bonding scheme can be inferred from the  $\text{O} \cdots \text{O}$  distances that involve either hydroxyl groups or  $\text{H}_2\text{O}$  molecules (Table 5). The bond-valence sums (BVSs) given in Table 4 provide important information that supports the assignment of the O sites to  $\text{O}^{2-}$  anions,  $(\text{OH})^-$  groups, or  $\text{H}_2\text{O}$  molecules. The BVSs for  $\text{H}_2\text{O}$  molecules are in the range of 0.00–0.59 valence units (v.u.), whereas BVSs for the  $\text{O}^{2-}$  anions (except  $\text{O}_{62}$  and  $\text{O}_{71}$ ) without

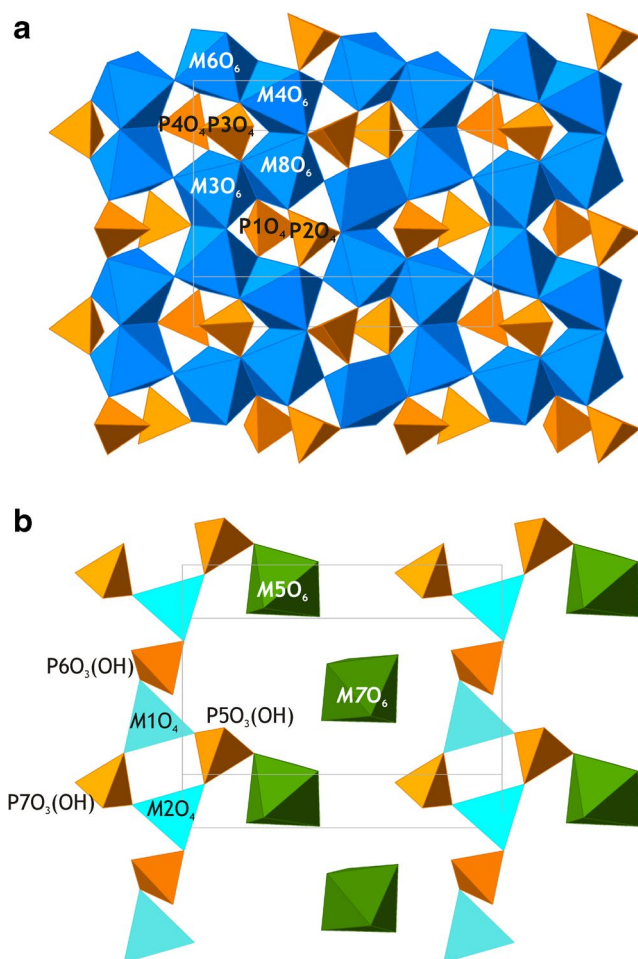
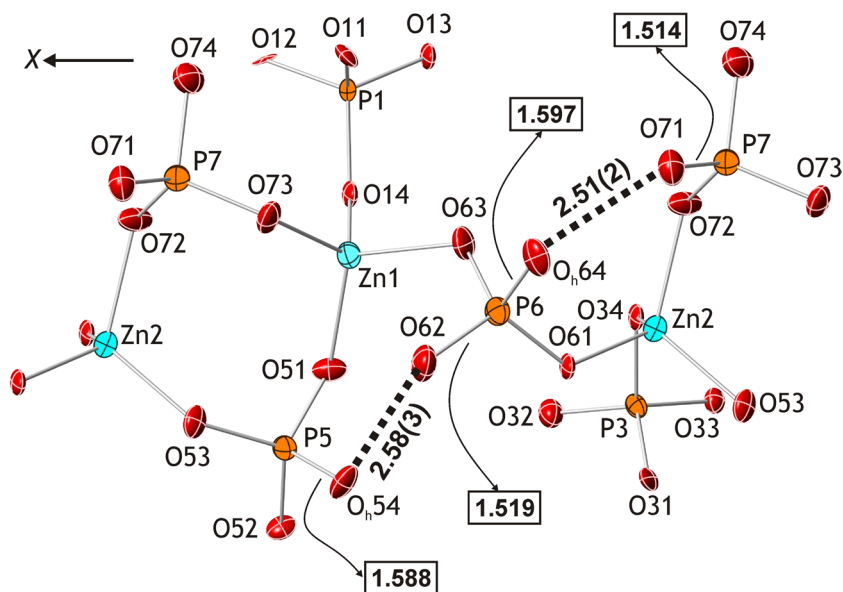


**Fig. 5** Projection of the **a** and **b** layers in the crystal structure of batagayite onto the (001) plane

**Fig. 6** The atomic configuration of the  $[\text{Zn}_2(\text{PO}_4)(\text{PO}_3\text{OH})_2]^-$  chains in the crystal structure of batagayite. The  $\text{O}\cdots\text{O}$  contacts corresponding to strong  $\text{O}-\text{H}\cdots\text{O}$  bonds are shown as bold dashed lines. The  $\text{P}-\text{O}$  bond lengths are given in boxes. See text for details



contributions from hydrogen bonds vary from 1.54 to 2.02 v.u. The BVSs for the  $\text{O}_{\text{h}54}$  and  $\text{O}_{\text{h}64}$  are equal to 1.24 and 1.32 v.u., which is typical for hydroxyl ions. The BVSs for the  $\text{O}_{62}$  and  $\text{O}_{71}$  sites are equal to 1.38 and 1.32 v.u., which would allow to consider them as hydroxyl ions too. However, both sites form rather short anion–anion contacts to the adjacent hydroxyl sites, forming the  $\text{O}_{\text{h}64}-\text{O}_{71}$  and  $\text{O}_{\text{h}54}-\text{O}_{62}$  pairs with the interatomic distances of 2.51(2) and 2.58(3) Å, respectively. These distances are rather short and indicate the formation of strong hydrogen bonds between respective  $(\text{OH})^-$  groups and O atoms. As it has been mentioned above, the  $\text{P}-\text{O}_{\text{h}64}$  and  $\text{P}-\text{O}_{\text{h}54}$  bonds are the longest  $\text{P}-\text{O}$  bonds in the  $\text{P6O}_4$  and  $\text{P5O}_4$  tetrahedra, respectively, whereas the  $\text{P7}-\text{O}_{71}$  and  $\text{P6}-\text{O}_{62}$  bond lengths are 1.514(18) and 1.519(18) Å, respectively. Therefore, the bond-valence deficiency observed for the  $\text{O}_{62}$  and  $\text{O}_{71}$  sites is compensated by the formation of strong hydrogen bonds to the  $\text{O}_{\text{h}54\text{H}}$  and  $\text{O}_{\text{h}64\text{H}}$  groups, respectively. The scheme of possible formation of these hydrogen bonds is shown in Fig. 6. It is worthy to note that the  $\text{O}_{\text{h}54}-\text{H}\cdots\text{O}_{62}$  and  $\text{O}_{\text{h}64}-\text{H}\cdots\text{O}_{71}$  bonds occur within tetrahedral chains formed by the  $(\text{M1O}_4)$ ,  $(\text{M2O}_4)$ ,  $(\text{P5O}_3\text{OH})$ ,  $(\text{P6O}_3\text{OH})$ , and  $(\text{P7O}_3\text{OH})$  tetrahedra (Fig. 5b).

### Powder diffraction

The powder X-ray diffraction pattern (Table 6) was obtained using a Rigaku R-Axis RAPID II diffractometer equipped with a cylindrical image plate detector using Debye–Scherrer geometry ( $d = 127.4$  mm;  $\text{CoK}\alpha$  radiation). The data were integrated using the software package



**Table 6** X-ray powder diffraction data for batagayite

$I_{\text{meas}}$	$d_{\text{meas}}, \text{\AA}$	$d_{\text{calc}}, \text{\AA}$	$hkl$	$I_{\text{meas}}$	$d_{\text{meas}}, \text{\AA}$	$d_{\text{calc}}, \text{\AA}$	$hkl$
<b>100</b>	<b>14.59</b>	14.60		001 1	2.473	2.473	241
1	7.01	7.01		110 6	2.439	2.440	312
6	6.83	6.84		101 <b>16</b>	<b>2.411</b>	2.412	044
5	6.64	6.65	$1\bar{1}\bar{1}$	7	2.389	2.391	016
<b>25</b>	<b>6.34</b>	6.35		012 5	2.272	2.276	026
<b>11</b>	<b>6.02</b>	6.04		111 2	2.247	2.247	135
3	5.88	5.88		021 5	2.160	2.161	045
5	5.38	5.40	$1\bar{1}\bar{2}$	2	2.085	2.086	007
1	5.11	5.10		120 3	2.074	2.075	160
<b>37</b>	<b>4.864</b>	4.869		003 1	2.013	2.012	$2\bar{4}\bar{5}$
<b>13</b>	<b>4.766</b>	4.771		112 2	1.9964	1.9951	$1\bar{2}\bar{7}$
6	4.679	4.683		121 1	1.9775	1.9777	162
2	4.541	4.553		013 4	1.9387	1.9393	$4\bar{2}\bar{3}$
1	4.369	4.369	$1\bar{2}\bar{2}$	1	1.8721	1.8728	127
1	3.992	3.983	$2\bar{1}\bar{1}$	4	1.8290	1.8264	403
5	3.815	3.814		130 5	1.8232	1.8227	$1\bar{1}\bar{8}$
8	3.690	3.691	$1\bar{2}\bar{3}$	2	1.7492	1.7494	217
6	3.635	3.631		131 2	1.7289	1.7295	172
3	3.468	3.478	$1\bar{3}\bar{2}$	4	1.6914	1.6910	$\bar{5}01$
3	3.413	3.417	$1\bar{1}\bar{4}$	4	1.6792	1.6796	038
2	3.294	3.291		132 2	1.6202	1.6202	057
7	3.214	3.214		040 4	1.6087	1.6089	$1\bar{6}\bar{6}$
<b>20</b>	<b>3.102</b>	3.104	$1\bar{2}\bar{4}$	5	1.5861	1.5849	521
4	2.999	2.993		230 1	1.5766	1.5774	218
5	2.938	2.941		042 2	1.5519	1.5519	$2\bar{4}\bar{8}$
5	2.908	2.908		133 1	1.5280	1.5279	531
3	2.847	2.848		015 6	1.4987	1.4991	$4\bar{3}\bar{7}$
8	2.820	2.823	$1\bar{1}\bar{5}$	1	1.4711	1.4709	084
<b>11</b>	<b>2.678</b>	2.679	$2\bar{3}\bar{3}$	4	1.4512	1.4512	0.11.0
5	2.635	2.639		105 2	1.4226	1.4227	176
2	2.580	2.580	$3\bar{2}\bar{1}$	2	1.4072	1.4076	524
6	2.547	2.548		240 1	1.3952	1.3945	600

Note: The eight strongest lines are highlighted bold

Osc2Tab/SQRay (Britvin et al. 2017). The unit-cell parameters refined from the powder data are as follows:  $P2_1$ ,  $a = 8.460(1)$ ,  $b = 12.852(1)$ ,  $c = 14.774(3)$  Å,  $\beta = 98.67(1)^\circ$ ,  $V = 1588.6(1)$  Å<sup>3</sup> and  $Z = 2$ , which are in good agreement with the single-crystal data (Table 3). The eight diagnostic lines in the X-ray powder-diffraction pattern are ( $I$ - $d$ [Å]- $hkl$ ): 100-14.59-001, 25-6.34-012, 11-6.02-111, 37-4.864-003, 13-4.766-112, 20-3.102- $1\bar{2}\bar{4}$ , 11-2.678- $2\bar{3}\bar{3}$ , 16-2.411-044.

## Discussion

From the crystal chemical point of view, batagayite is a new member of the group of minerals and inorganic compounds based upon the  $[M(TO_4)\phi]$  layers of the type shown in Fig. 5a. Table 7 provides the list of compounds that belong to this group together with their crystallographic parameters. Among these compounds, batagayite is the only example of a structure containing other modules along the  $[M(TO_4)\phi]$  layers. A detailed analysis of structural

**Table 7** Minerals and inorganic compounds with  $[M(\text{TO}_4)\phi]$  layers ( $M = \text{Fe, Mg, Mn, Ni, Zn, Co}$ ;  $T = \text{P, As}$ ;  $\phi = \text{OH, H}_2\text{O}$ )

Mineral	Chemical formula	Space group	<i>a</i> , Å	<i>b</i> , Å /	<i>c</i> , Å	<i>V</i> , Å <sup>3</sup>	$\beta$ , deg.	Ref.
Angarfit	$\text{NaFe}^{3+}_5(\text{PO}_4)_4(\text{OH})_4 \cdot 4\text{H}_2\text{O}$	<i>C</i> 222 <sub>1</sub>	<b>12.800</b>	17.908	<b>8.211</b>	1882.2	90	1
Bakhchisaraitsevite	$\text{Na}_2\text{Mg}_5(\text{PO}_4)_4 \cdot 7\text{H}_2\text{O}$	<i>P</i> 2 <sub>1</sub> / <i>c</i>	<b>8.309</b>	<b>12.906</b>	17.486	1834.0	102.0	2
Batagayite	$\text{CaZn}_2(\text{Zn,Cu})_6(\text{PO}_4)_4(\text{PO}_3\text{OH})_3 \cdot 12\text{H}_2\text{O}$	<i>P</i> 2 <sub>1</sub>	<b>8.426</b>	<b>12.831</b>	14.693	1571.1	98.5	3
Castellaroite	$\text{Mn}^{2+}_3(\text{AsO}_4)_2 \cdot 4.5\text{H}_2\text{O}$	<i>P</i> 2 <sub>1</sub> / <i>n</i>	<b>8.757</b>	<b>13.468</b>	18.652	2191.7	94.9	4
Mejillonesite	$\text{NaMg}_2(\text{PO}_3\text{OH})(\text{PO}_4)(\text{OH}) \cdot \text{H}_5\text{O}_2$	<i>P</i> <i>bca</i>	16.295	<b>13.009</b>	<b>8.434</b>	1787.9	90	5
Metaswitzerite	$\text{Mn}_3(\text{PO}_4)_2 \cdot 4\text{H}_2\text{O}$	<i>P</i> 2 <sub>1</sub> / <i>c</i>	<b>8.496</b>	<b>13.173</b>	17.214	1913.6	96.7	6
Rimkorolgit	$\text{BaMg}_5(\text{PO}_4)_4 \cdot 8\text{H}_2\text{O}$	<i>P</i> 2 <sub>1</sub> / <i>c</i>	<b>8.335</b>	<b>12.830</b>	18.313	1958.5	90.0	7
Switzerite	$\text{Mn}_3(\text{PO}_4)_2 \cdot 7\text{H}_2\text{O}$	<i>P</i> 2 <sub>1</sub> / <i>a</i>	<b>8.528</b>	<b>13.166</b>	11.812	1245.9	110.1	8
–	$\text{Na}(\text{H}_3\text{O})_2\text{Ni}_4(\text{PO}_4)_3(\text{PO}_2(\text{OH})_2)(\text{OH})_4$	<i>P</i> 2 <sub>1</sub>	<b>8.374</b>	<b>12.810</b>	8.407	866.1	106.2	9
–	$(\text{H}_3\text{O})\text{Co}_2(\text{PO}_3\text{OH})(\text{PO}_2(\text{OH})_2)(\text{OH})_2$	<i>Pcab</i>	<b>8.443</b>	<b>13.093</b>	15.484	1711.7	90	9

References: (1) Kampf et al. 2012; (2) Yakubovich et al. 2000; (3) this work; (4) Kampf et al. 2016; (5) Atencio et al. 2012; (6) Fanfani and Zanazzi 1979; (7) Krivovichev et al. 2002; (8) Zanazzi et al. 1986; (9) Hamanaka and Imoto 1998

Note: Unit-cell dimensions with the layers are highlighted in bold

complexity of the group is given elsewhere (Krivovichev SV (2018) Ladders of information: what contributes to the structural complexity of inorganic crystals. *Z Kristallogr*, accepted).

Batagayite is the secondary low-temperature mineral formed as a result of alteration of primary minerals such as native copper and apatite. Its low-temperature formation is in good agreement with its structural complexity parameters, calculated following the procedure suggested by Krivovichev (2012, 2013) as:  $\nu = 112$ ,  $I_G = 5.807$  bits/atom,  $I_{G,\text{total}} = 650.424$  bits/cell (without contributions from H atoms), and  $\nu = 166$ ,  $I_G = 6.375$  bits/atom,  $I_{G,\text{total}} = 1058.257$  bits/cell (taking into account contributions from H atoms introduced as surrogate atoms by H-correction; see Pankova et al. (2018) for details) (herein  $\nu$  is the number of atoms per reduced unit cell, and  $I_G$  and  $I_{G,\text{total}}$  are the amounts of the structural information per atom and per reduced unit cell, respectively). Therefore batagayite should be considered as a very complex mineral according to the classification proposed by Krivovichev (2013, 2014). It is of interest that batagayite is closely associated with sampleite,  $\text{NaCaCu}_5(\text{PO}_4)_4\text{Cl} \cdot 5\text{H}_2\text{O}$ , structural complexity of which is measured as  $I_{G,\text{total}} = 665.86$  bits/cell. Another Cu phosphate in association with batagayite is epifanovite,  $\text{NaCaCu}_5(\text{PO}_4)_4[\text{AsO}_2(\text{OH})_2] \cdot 7\text{H}_2\text{O}$  (Yakovenchuk et al. 2017; Panikorovskii et al. 2017), that has 303.050 bits/cell only. Therefore, with these complexity parameters sampleite and epifanovite should be considered as complex and intermediate in complexity, respectively. The reason for the higher complexity of batagayite is obviously the modular character of its structure, which contains different building blocks such as octahedral-tetrahedral layers and tetrahedral chains. In general, the high structural complexity of secondary phosphates is typical for low-temperature minerals and, at least in part, is controlled by their high hydration states.


**Acknowledgements** The manuscript was essentially improved following reviews by Anthony R. Kampf and Gerald Giester, and editorial efforts of Maarten A.T.M. Broekmans. This research was supported by the Russian Science Foundation, grant 14-17-00071.

## References

- Agilent Technologies (2014) CrysAlis CCD and CrysAlis RED. Oxford Diffraction Ltd, Yarnton, Oxfordshire
- Atencio D, Chukanov NV, Nestola F, Witzke T, Coutinho JMV, Zadov AE, Contreira Filho RR, Färber G (2012) Mejillonesite, a new acid sodium, magnesium phosphate mineral, from Mejillones, Antofagasta, Chile. *Amer Mineral* 97:19–25
- Britvin SN, Dolivo-Dobrovolsky DV, Krzhizhanovskaya MG (2017) Software for processing of X-ray powder diffraction data obtained from the curved image plate detector of Rigaku RAXIS Rapid II diffractometer. *Zap Ross Mineral Obsh*, in press
- Fanfani L, Zanazzi PF (1979) Switzerite: its chemical formula and crystal structure. *Tscherm Mineral Petrogr Mitt* 26:255–269
- Ferraris G, Ivaldi G (1984) X-OH and O-H...O bond lengths in protonated oxoanions. *Acta Crystallogr B* 40:1–6
- Frost RL (2004) An infrared and Raman spectroscopic study of natural zinc phosphates. *Spectrochim Acta A* 60:1439–1445
- Frost RL, Bouzaid JM, Reddy BJ (2007) Vibrational spectroscopy of the sorosilicate mineral hemimorphite  $\text{Zn}_4(\text{OH})_2\text{Si}_2\text{O}_7 \cdot \text{H}_2\text{O}$ . *Polyhedron* 26:2405–2412
- Frost RL, Scholz R, Lypez A, Xi Y (2014) A vibrational spectroscopic study of the phosphate mineral whiteite  $\text{CaMn}^{2+}\text{Mg}_2\text{Al}_2(\text{PO}_4)_4(\text{OH})_2 \cdot 8(\text{H}_2\text{O})$ . *Spectrochim Acta Mol Biomol Spectrosc* 124:243–248
- Gagné OC, Hawthorne FC (2015) Comprehensive derivation of bond-valence parameters for ion pairs involving oxygen. *Acta Crystallogr B* 71:562–578
- Giester G, Kolitsch U, Leverett P, Turner P, Williams PA (2007) The crystal structures of lavendulan, sampleite, and a new polymorph of sampleite. *Eur J Mineral* 19:75–93
- Hamanaka N, Imoto H (1998) Syntheses, structures, and magnetic properties of metal(II) phosphates with  $[\text{M}(\text{OH})(\text{PO}_4)]^{2-}$  layers ( $M = \text{Ni, Co, Mg}$ ). *Inorg Chem* 37:5844–5850

- Huminicki DMC, Hawthorne FC (2002) The crystal chemistry of phosphate minerals. *Rev Mineral Geochem* 48:123–254
- Ivanov VV, Pyatenko YuA (1959) On so-called kesterite. *Zap Vses Mineral Obshch* 88:165–168 in (Russian)
- Jahn HA, Teller E (1937) Stability of polyatomic molecules in degenerate electronic states. I. Orbital degeneracy. *Proc Roy Soc A* 161:220–235
- Kampf AR, Mills SJ, Housley RM, Favreau G, Boulliard JC, Bourgoin V (2012) Angarfite, a new mineral species from the Angarf-Sud pegmatite, Morocco: description and crystal structure. *Can Mineral* 50:781–791
- Kampf AR, Cámara F, Ciriotti ME, Nash BP, Balestra C, Chiappino L (2016) Castellarite,  $\text{Mn}^{2+}_3(\text{AsO}_4)_2 \cdot 4.5\text{H}_2\text{O}$ , a new mineral from Italy related to metaswitzerite. *Eur J Mineral* 28:687–696
- Kokunin MV (2011) Rare minerals of the forgotten deposit. *Otechestvennaya Geologiya* 2011(1):72–82 (Russian)
- Krivovichev SV (2012) Topological complexity of crystal structures: quantitative approach. *Acta Crystallogr A* 68:393–398
- Krivovichev SV (2013) Structural complexity of minerals: information storage and processing in the mineral world. *Mineral Mag* 77:275–326
- Krivovichev SV (2014) Which inorganic structures are the most complex? *Angew Chem Int Ed* 53:654–661
- Krivovichev SV, Britvin SN, Burns PC, Yakovenchuk VN (2002) Crystal structure of rimkorolite,  $\text{Ba}[\text{Mg}_5(\text{H}_2\text{O})_7(\text{PO}_4)_4](\text{H}_2\text{O})$ , and its comparison with bakhchisaraitsevite. *Eur J Mineral* 14:397–402
- Liu X, Feng Y, Cui H, Liu F, Hao X, Conibeer G, Mitzi DB, Green M (2016) The current status and future prospects of kesterite solar cells: a brief review. *Prog Photovolt Res Appl* 24:879–898
- Panikorovskii TL, Krivovichev SV, Yakovenchuk VN, Ivanyuk GYu (2017) The crystal structure of epifanovite. *Zap Ross Mineral Obshch*, in press (in Russian)
- Pankova YA, Gorelova LA, Krivovichev SV, Pekov IV (2018) The crystal structure of ginorite,  $\text{Ca}_2[\text{B}_{14}\text{O}_{20}(\text{OH})_6](\text{H}_2\text{O})_5$ , and the analysis of dimensional reduction and structural complexity in the  $\text{CaO-B}_2\text{O}_3\text{-H}_2\text{O}$  system. *Eur J Mineral* accepted. <https://doi.org/10.1127/ejm/2018/0030-2695>
- Rudolph WW, Irmer G (2007) Raman and infrared spectroscopic investigations on aqueous alkali metal phosphate solutions and density functional theory calculations of phosphate–water clusters. *Appl Spectrosc* 61:1312–1327
- Sheldrick GM (2008) A short history of SHELX. *Acta Crystallogr A* 64:112–122
- Yakovenchuk VN, Pakhomovsky YaA, Konoplyova NG, Panikorovskii TL, Mikhailova YuA, Bocharov VN, Krivovichev SV, Ivanyuk GYu (2017) Epifanovite,  $\text{NaCaCu}_5(\text{PO}_4)_4[\text{AsO}_2(\text{OH})_2] \cdot 7\text{H}_2\text{O}$ , a new mineral from the Kester deposit (Sakha-Yakutia, Russia). *Zap Ross Mineral Obshch*, in press (in Russian)
- Yakubovich OV, Massa W, Liferovich RP, Pakhomovsky YaA (2000) The crystal structure of bakhchisaraitsevite,  $[\text{Na}_2(\text{H}_2\text{O})_2]\{(\text{Mg}_{4.5}\text{Fe}_{0.5})(\text{PO}_4)_4(\text{H}_2\text{O})_5\}$ , a new mineral species of hydrothermal origin from the Kovdor phoscorite-carbonatite Complex, Russia. *Can Mineral* 38:831–838
- Zanazzi PF, Leavens PB, White JS (1986) Crystal structure of switzerite,  $\text{Mn}_3(\text{PO}_4)_2 \cdot 7\text{H}_2\text{O}$ , and its relationship to metaswitzerite,  $\text{Mn}_3(\text{PO}_4)_2 \cdot 4\text{H}_2\text{O}$ . *Amer Mineral* 71:1224–1228

## Affiliations

Victor N. Yakovenchuk<sup>1</sup> · Yakov A. Pakhomovsky<sup>1</sup> · Nataliya G. Konopleva<sup>1</sup> · Taras L. Panikorovskii<sup>1,2</sup> · Ayya Bazai<sup>1</sup> · Julia A. Mikhailova<sup>1</sup> · Vladimir N. Bocharov<sup>3</sup> · Gregory Yu. Ivanyuk<sup>1</sup> · Sergey V. Krivovichev<sup>1,2</sup> 

<sup>1</sup> Nanomaterials Research Centre, Kola Science Centre, Russian Academy of Sciences, 14 Fersman Street, Apatity 184200, Russia

<sup>2</sup> Department of Crystallography, St. Petersburg State University, 7–9 University Emb, St. Petersburg 199034, Russia

<sup>3</sup> Geo Environmental Centre “Geomodel”, St. Petersburg State University, Ul’yanovskaya Str., St. Petersburg 198504, Russia